

Gravitational Lensing by Phantom Black holes

Galin N. Gyulchev^{1*}, Ivan Zh. Stefanov^{2†}

¹ *Department of Physics, Biophysics and Roentgenology, Faculty of Medicine, Snt. Kliment Ohridski University of Sofia, 1, Kozyak Str., 1407 Sofia, Bulgaria*

² *Department of Applied Physics, Technical University of Sofia, 8, Snt. Kliment Ohridski Blvd., 1000 Sofia, Bulgaria*

Abstract

In some models dark energy is described by phantom scalar fields (scalar fields with "wrong" sign of the kinetic term in the lagrangian). In the current paper we study the effect of phantom scalar field and/or phantom electromagnetic field on gravitational lensing by black holes in the strong deflection regime. The black-hole solutions that we have studied have been obtained in the frame of the Einstein-(anti-)Maxwell-(anti-)dilaton theory. The obtained results show considerable effect of the phantom scalar and electromagnetic fields on the angular position, brightness and separation of the relativistic images.

PACS numbers: 95.30.Sf, 04.20.Dw, 04.70.Bw, 98.62.Sb

Keywords: Relativity and gravitation; Gravitational lensing; Classical black holes; Phantom black holes; Einstein-Maxwell-dilaton theory; Dark energy

*email: gyulchev@phys.uni-sofia.bg

†email: izhivkov@tu-sofia.bg

1 Introduction

Modern observational programs including type Ia SNe, cosmic microwave background anisotropy and mass power spectrum suggest that the universe is dominated by mysterious matter termed dark energy (DE) which has negative pressure and violates the energy conditions [2, 3, 1]. Considerable efforts are made to study the nature of DE. Different effective models of dark energy have been proposed in literature (See [4] and [5] for recent exhaustive reviews). In some of them the possibility of describing DE by phantom fields is considered.

The natural questions whether local manifestations of DE at astrophysical scale can be observed. Exact solutions describing neutron stars containing DE have obtained in [6]. There have been also some recent efforts in that direction. In [7] the effect of DE on the structure and on the spectrum of quasinormal frequencies of neutron stars has been studied. Mixed stars containing both dark energy and ordinary matter have been presented in a number of papers (See [6] and references therein). Solutions describing black holes coupled to phantom fields have also been found. To our knowledge the first solutions of phantom black holes have been obtained by Gibbons and Rasheed [8]. These solutions were later elaborated by Clément et al. [9, 10] and Gao Zhang [11] for higher dimensions. Regular black holes coupled to phantom scalar field have been reported by Bronnikov [12]. Recent interest in phantom black holes have been connected with the study of their thermodynamics and the possibility of phase transitions [13, 14], the study of gravitational collapse of a charged scalar field [15] and the study of light paths in such space-times [16].

As we have already mentioned gravitational waves and the frequencies of quasinormal ringing in particular can provide rich information for the structure of compact astrophysical objects and thus can serve as a powerful tool for studying of the local manifestation of DE. Another possibility could be provided by gravitational lensing especially in the strong deflection regime. There has been considerable effort for the theoretical study of gravitational lensing in the strong deflection regime (For more details on the matter we refer the reader to [17] and references therein). In his papers [18, 19] Bozza proposed a method for the calculation of the deflection angle in the regime of strong deflection in the particular case when both the observer and the gravitational source lie in the equatorial plane. Since then it has been applied to study the gravitational lensing caused by different exotic, compact objects. The particular cases in which both the scalar field and the electromagnetic field have canonical form, i.e. the EMD black hole has been already reported by Bhadra [20]. The lensing by EMD black holes with de-Sitter and anti-de-Sitter asymptotics have been studied by [21] and [22], respectively. In the last two cases the scalar field has a non zero potential. Lensing in the strong field regime by black holes coupled to electromagnetic field has been considered also in [23, 24, 25, 26, 27, 28].

Black holes with opposite sign of the charge term in the metric (as in the case of anti-Reissner Nordström black hole) have been applied to model the object in the center of our galaxy – Sgr A* and their lensing has been studied in [29] and [30]. In these black holes, however, the charge is tidal and does not have electromagnetic origin. Lensing by black holes with tidal charge gas been also considered in [31].

One of the aims of the current paper is to study the effect of phantom scalar field (phantom dilaton) on gravitational lensing. In the presence of exotic matter such as phantom

fields wormholes may exist. Lensing by different wormholes, for example the Ellis's and the Janis-Newman-Winicour's (JNW) wormholes, has attracted significant research interest [32]–[43]. JNW naked singularities (naked singularities coupled to canonical massless scalar field) acting as gravitational lens have been considered by Virbhadra et al. [44, 45, 46]. The lensing of the JNW solution in the context of scalar-tensor theories has been studied by Bhadra [47]. Generalization with inclusion of rotation has been made in [48].

Our goal is apply the apparatus of gravitational lensing by black holes in the strong deflection limit to study the possible local manifestation of dark energy. For this purpose we model DE with phantom dilaton and phantom electromagnetic field. We compare the characteristics of relativistic images of four black holes: the standard Einstein-Maxwell black hole (EMD); the Einstein-anti-Maxwell-dilaton black hole which has a phantom electromagnetic field ($\overline{\text{EMD}}$)[†]; the Einstein-Maxwell-anti-dilaton black hole which has a phantom dilaton ($\overline{\text{EMD}}$); and the Einstein-anti-Maxwell-anti-dilaton black hole in which both the dilaton and the electromagnetic field are phantom ($\overline{\overline{\text{EMD}}}$).

2 Phantom black holes

When phantom dilaton and/or phantom electromagnetic field is considered the action of Einstein-Maxwell-dilaton theory is generalized to the following form

$$S = \int dx^4 \sqrt{-g} \left[R - 2\eta_1 g^{\mu\nu} \nabla_\mu \varphi \nabla_\nu \varphi + \eta_2 e^{-2\alpha\varphi} F^{\mu\nu} F_{\mu\nu} \right]. \quad (1)$$

R denotes the Ricci scalar curvature, φ is the dilaton, F is the Maxwell tensor and the constant α determines the coupling between the dilaton and the electromagnetic field. For the usual dilaton the dilaton-gravity coupling constant η_1 takes the value $\eta_1 = 1$ while for phantom dilaton $\eta_1 = -1$. Similarly, the Maxwell-gravity coupling constant η_2 takes the values $\eta_2 = 1$ and $\eta_2 = -1$ in the Maxwell and anti-Maxwell case, respectively.

2.1 Einstein Maxwell Dilaton black holes

The line element of the EMD black hole is

$$ds^2 = - \left(1 - \frac{r_+}{r}\right) \left(1 - \frac{r_-}{r}\right)^\gamma dt^2 + \left(1 - \frac{r_+}{r}\right)^{-1} \left(1 - \frac{r_-}{r}\right)^{-\gamma} dr^2 + r^2 \left(1 - \frac{r_-}{r}\right)^{1-\gamma} (d\theta^2 + \sin^2 \theta d\phi^2), \quad (2)$$

where the parameter $\gamma = (1 - \alpha^2)/(1 + \alpha^2)$ has been introduced for convenience. It varies in the interval $[-1, 1]$ for $\alpha \in (-\infty, \infty)$. The solutions for the dilaton and the Maxwell field are

$$e^{2\alpha\varphi} = \left(1 - \frac{r_-}{r}\right)^{1-\gamma}, \quad F = \frac{Q}{r^2} dt \wedge dr \quad (3)$$

For the magnetically charged solution the metric is the same but the sign of the scalar field φ must be reversed and the Maxwell field becomes $F = P \sin \theta d\theta \wedge d\phi$. The parameters r_+

[†]We will adopt the abbreviations introduced in [8].

and r_- are interpreted as an event horizon and an inner Cauchy horizon, respectively. The ADM mass M and the charge Q can be expressed by r_+ and r_-

$$2M = r_+ + \gamma r_-, \quad 2Q^2 = (1 + \gamma)r_+ r_-. \quad (4)$$

Relations (4) can be inverted to express the horizons in terms of the ADM mass M and the charge Q

$$r_+ = M \left[1 + \sqrt{1 - \frac{2\gamma}{1 + \gamma} \left(\frac{Q}{M} \right)^2} \right], \quad r_- = \frac{M}{\gamma} \left[1 - \sqrt{1 - \frac{2\gamma}{1 + \gamma} \left(\frac{Q}{M} \right)^2} \right] \quad (5)$$

The equation for r_+ (or r_-) obtained from (4) is biquadratic. The solutions are grouped in two couples. The couple which contains the largest of all four roots is chosen. The same choice is made in the other three classes of solutions considered in this paper. The two horizons merge at

$$\left(\frac{Q}{M} \right)^2 = \left(\frac{Q}{M} \right)_{\text{crit}}^2 = \frac{2}{1 + \gamma} \quad (6)$$

and for lower values of $(Q/M)^2$ the solution describes a naked singularity. In the limit $\gamma \rightarrow 1$ the solution restores the Reissner-Nordström black hole.

2.2 Einstein anti-Maxwell Dilaton black holes

In the case of $\overline{\text{EMD}}$ black hole the line element is again (2). The solutions for the dilaton and the anti-Maxwell field are

$$e^{2\alpha\varphi} = \left(1 - \frac{r_-}{r} \right)^{1-\gamma}, \quad F = -\frac{Q}{r^2} dt \wedge dr \quad (7)$$

The ADM mass M and the anticharge Q are

$$2M = r_+ + \gamma r_-, \quad 2Q^2 = -(1 + \gamma)r_+ r_-. \quad (8)$$

The ‘‘horizons’’ expressed in terms of the ADM mass M and the anticharge Q are

$$r_+ = M \left[1 + \sqrt{1 + \frac{2\gamma}{1 + \gamma} \left(\frac{Q}{M} \right)^2} \right], \quad r_- = \frac{M}{\gamma} \left[1 - \sqrt{1 + \frac{2\gamma}{1 + \gamma} \left(\frac{Q}{M} \right)^2} \right] \quad (9)$$

The parameter r_+ is positive and is interpreted as an event horizon while r_- is a negative and can be considered as a singularity which is never reached since the singularity at $r = 0$ is reached before that. Hence, these black holes have the same causal structure as the Schwarzschild black hole. Again, there is restriction for the parameter (Q/M)

$$\left(\frac{Q}{M} \right)^2 \leq \left(\frac{Q}{M} \right)_{\text{crit}}^2 = -\frac{1 + \gamma}{2\gamma}. \quad (10)$$

The limit $\gamma \rightarrow 1$ corresponds to the anti-Reissner-Nordström black hole (a Reissner-Nordström black hole black hole with imaginary charge). (Q/M) is unbound for positive γ .

2.3 Einstein Maxwell anti-Dilaton black holes

The line element of the EMD black hole is

$$ds^2 = - \left(1 - \frac{r_+}{r}\right) \left(1 - \frac{r_-}{r}\right)^{1/\gamma} dt^2 + \left(1 - \frac{r_+}{r}\right)^{-1} \left(1 - \frac{r_-}{r}\right)^{-1/\gamma} dr^2 + r^2 \left(1 - \frac{r_-}{r}\right)^{1-1/\gamma} (d\theta^2 + \sin^2 \theta d\phi^2), \quad (11)$$

The solutions for the dilaton and the Maxwell field are

$$e^{2\alpha\varphi} = \left(1 - \frac{r_-}{r}\right)^{1-1/\gamma}, \quad F = \frac{Q}{r^2} dt \wedge dr \quad (12)$$

When $\gamma > 0$, $0 \leq r_- \leq r_+$, so the causal structure is the same as for the EMD case. For $\gamma < 0$, however, $r_- \leq 0 \leq r_+$ and the black hole has the same causal structure as in the EMD case. The ADM mass M and the charge Q are expressed by r_+ and r_- in the following way

$$2M = r_+ + \frac{1}{\gamma} r_-, \quad 2Q^2 = \frac{(1+\gamma)}{\gamma} r_+ r_-. \quad (13)$$

Relations (13) can be inverted to express the ‘‘horizons’’ in terms of the ADM mass M and the charge Q

$$r_+ = M \left[1 + \sqrt{1 - \frac{2}{1+\gamma} \left(\frac{Q}{M}\right)^2} \right], \quad r_- = \gamma M \left[1 - \sqrt{1 - \frac{2}{1+\gamma} \left(\frac{Q}{M}\right)^2} \right]. \quad (14)$$

For r_+ and r_- to be real the following relation must hold

$$\left(\frac{Q}{M}\right)^2 \leq \left(\frac{Q}{M}\right)_{\text{crit}}^2 = \frac{1+\gamma}{2}. \quad (15)$$

Here in the limit $\gamma \rightarrow 1$ the Reissner-Nordström black hole is restored.

2.4 Einstein anti-Maxwell anti-Dilaton black holes

In the case of EMD black hole the line element is given again by (11). The solutions for the dilaton and the anti-Maxwell field are

$$e^{2\alpha\varphi} = \left(1 - \frac{r_-}{r}\right)^{1-1/\gamma}, \quad F = -\frac{Q}{r^2} dt \wedge dr \quad (16)$$

When $\gamma > 0$, $r_- \leq 0 \leq r_+$ and the causal structure is Schwarzschild-like. For $\gamma < 0$, however, $0 \leq r_- \leq r_+$ and the black hole has two horizons, an event horizon and an inner Cauchy horizon. The ADM mass M and the anticharge Q are

$$2M = r_+ + \frac{1}{\gamma} r_-, \quad 2Q^2 = -\frac{(1+\gamma)}{\gamma} r_+ r_-. \quad (17)$$

Relations (17) can be inverted to express the “horizons” in terms of the ADM mass M and the charge Q

$$r_+ = M \left[1 + \sqrt{1 + \frac{2}{1+\gamma} \left(\frac{Q}{M} \right)^2} \right], \quad r_- = \gamma M \left[1 - \sqrt{1 + \frac{2}{1+\gamma} \left(\frac{Q}{M} \right)^2} \right]. \quad (18)$$

Unlike all three cases discussed above in the current case there are no restrictions for $(Q/M)^2$. The limit $\gamma \rightarrow 1$ corresponds, again, to the anti-Reissner-Nordström black hole.

3 Gravitational lensing in the strong field limit

Following Bozza’s notation we can express the metric of the general static spherically symmetric space-time in the form

$$ds^2 = A(x)dt^2 - B(x)dx^2 - x^2(d\theta^2 + \sin^2\theta d\varphi^2) \quad (19)$$

where we have introduced the new variable $x = r/M$. The deflection angle can be expressed as

$$\alpha(x_0) = I(x_0) - \pi \quad (20)$$

where

$$I(x_0) = 2 \int_{x_0}^{\infty} \frac{\sqrt{B(x)}}{\sqrt{C(x)} \sqrt{\frac{C(x)A(x_0)}{C(x_0)A(x)} - 1}} dx \quad (21)$$

and here x_0 represents the minimum distance from the photon trajectory to the gravitational source. The deflection angle diverges when the denominator of the above expression turns to zero i.e. at the points where the following relation $\frac{C'(x)}{C(x)} = \frac{A'(x)}{A(x)}$ holds. We use prime $(..)'$ to denote the derivative with respect to x . The largest root of this equation gives the radius of the photon sphere. For more details on photon surfaces we refer the reader to [49]

Here and bellow the following convention has been chosen $F_m = F|_{r_0=r_m}$ where F is an arbitrary quantity.

According to Bozza’s method [18, 19] the integral (21) is split in two parts – regular $I_R(x_0)$ and divergent $I_D(x_0)$

$$I(x_0) = I_D(x_0) + I_R(x_0). \quad (22)$$

In explicit form

$$I_D(x_{ps}) = \int_0^1 \frac{u_{ps}}{\sqrt{\beta_{ps}}} \sqrt{\frac{B_{ps}}{C_{ps}} \frac{x_{ps}}{\eta}} d\eta, \quad (23)$$

$$I_R(x_{ps}) = \int_0^1 \left[u_{ps} \sqrt{\frac{B(\eta)}{C(\eta)}} [R(\eta, u_{ps})]^{-1/2} \frac{x_{ps}}{(1-\eta)^2} - \frac{u_{ps}}{\sqrt{\beta_{ps}}} \sqrt{\frac{B_{ps}}{C_{ps}} \frac{x_{ps}}{\eta}} \right] d\eta. \quad (24)$$

In this formulas the following quantities have been introduced. The new variable

$$\eta = 1 - \frac{x_{ps}}{x_0}, \quad (25)$$

facilitates the numerical integration since it maps the open interval $[x_{ps}, \infty)$ to the closed interval $[0, 1]$. The function

$$R(\eta, u_{ps}) = \frac{C(\eta)}{A(\eta)} - u_{ps}^2 \quad (26)$$

is responsible for the divergence of the integrand. As the photon sphere is approached, i.e. when $\eta \rightarrow 0$ the leading order term of the integrand is $(\sqrt{\beta_{ps}\eta})^{-1}$. The coefficient in the expansion is

$$\beta_{ps} = \frac{1}{2} x_{ps}^2 \frac{C''_{ps} A_{ps} - C_{ps} A''_{ps}}{A_{ps}^2}. \quad (27)$$

The expansion shows that divergence of the deflection angle is logarithmic [18, 19]

$$\alpha(\theta) = -a \ln \left(\frac{\theta D_{OL}}{u_{ps}} - 1 \right) + b + O(u - u_{ps}). \quad (28)$$

where D_{OL} denotes the distance between observer and gravitational lens. The impact parameter is

$$u_{ps} = \sqrt{\frac{C_{ps}}{A_{ps}}}. \quad (29)$$

The strong field limit coefficients a and b are expressed as,

$$a = x_{ps} \sqrt{\frac{B_{ps}}{A_{ps} \beta_{ps}}}, \quad (30)$$

$$b = -\pi + I_R(x_{ps}) + a \ln \left(\frac{2\beta_{ps}}{u_{ps}^2} \right). \quad (31)$$

We will be interested also in the following observables. The angular separation between the lens and the n -th relativistic image

$$\theta_n^{pro} = \theta_n^0 \left(1 - \frac{u_{ps} \epsilon_n^{pro} (D_{OL} + D_{LS})}{a D_{OL} D_{LS}} \right), \quad (32)$$

where

$$\theta_n^0 = \frac{u_{ps}}{D_{OL}} (1 + \epsilon_n^{pro}), \quad \epsilon_n^{pro} = e^{\frac{b-2\pi n}{a}}. \quad (33)$$

D_{LS} is the lens-source distance, D_{OL} is the observer-lens distance. We are considering only prograde photons and this is what *pro* stands for. It is usually considered that only the first relativistic image can be observed separately and all other relativistic images would be packed together at angular position θ_∞ . The angular separation between the first relativistic image and the rest of the relativistic images is

$$s_1^{pro} = \theta_1 - \theta_\infty = \theta_\infty e^{\frac{b-2\pi}{a}}. \quad (34)$$

The third observable that is usually considered is the ratio between the magnitude of the first image μ_1 and the total magnitude of all other relativistic images $\sum_{n=2}^{\infty} \mu_n$

$$r = \frac{\mu_1}{\sum_{n=2}^{\infty} \mu_n} = e^{\frac{2\pi}{a}}, \quad (35)$$

which in terms of stellar magnitudes is

$$r_m = 2.5 \lg(r). \quad (36)$$

3.1 Photon sphere

For both solutions with canonical scalar field, EMD and $\overline{\text{EMD}}$, the expression for the photon sphere is

$$x_{ps} = \frac{3}{4}x_+ + \frac{1}{4}(2\gamma + 1)x_- + \frac{1}{4}\sqrt{9x_+^2 + (2\gamma + 1)^2 x_-^2 - 2(2\gamma + 5)x_+x_-}, \quad (37)$$

where $x_+ = r_+/M$ and $x_- = r_-/M$, r_+ and r_- are the parameters of the corresponding black-hole solution. The photon sphere x_{ps} , the event horizon x_+ and the inner horizon x_- of the EMD and $\overline{\text{EMD}}$ black holes are displayed on Fig. 1. In the EMD case for $\gamma < 0$ the photon sphere and the event horizon merge when $(Q/M) = (Q/M)_{\text{crit}}$. This situation has been recently discussed in [50]. In the $\overline{\text{EMD}}$ case we can see that (Q/M) is restricted from above only when $\gamma < 0$. The photon sphere and the event horizon do not merge for any value of (Q/M) in this case. The inner "horizon" x_- is behind the central singularity and is not present on the figure.

For the solutions with phantom scalar field, $\overline{\text{EMD}}$ and $\overline{\overline{\text{EMD}}}$, the photon sphere takes the form

$$x_{ps} = \frac{3}{4}x_+ + \frac{1}{4}\left(\frac{2}{\gamma} + 1\right)x_- + \frac{1}{4}\sqrt{9x_+^2 + \left(\frac{2}{\gamma} + 1\right)^2 x_-^2 - 2\left(\frac{2}{\gamma} + 5\right)x_+x_-}, \quad (38)$$

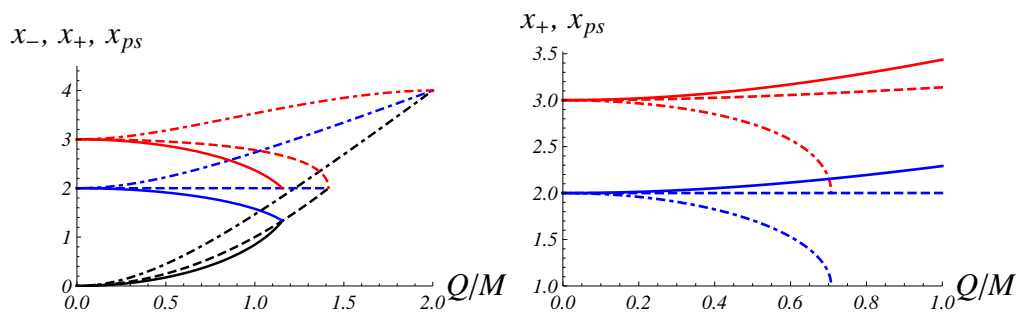


Figure 1: The photon sphere x_{ps} (red), the event horizon x_+ (blue) and the inner horizon x_- (black) of the EMD and $\overline{\text{EMD}}$ black holes for three values of γ : $\gamma = -0.5$ (dash-dot), $\gamma = 0$ (dash) and $\gamma = 0.5$ (solid).

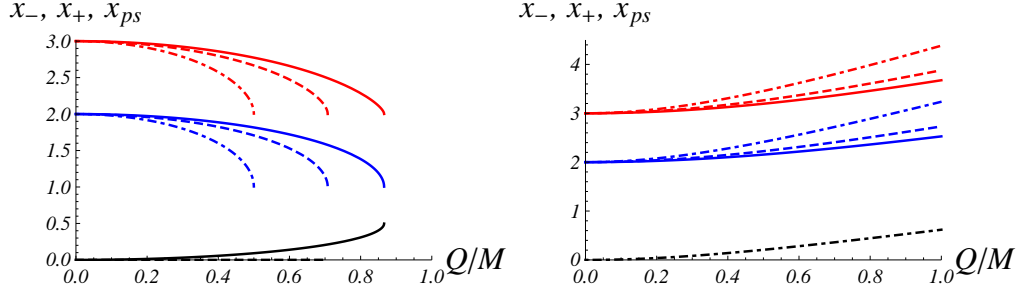


Figure 2: The photon sphere x_{ps} (red), the event horizon x_+ (blue) and the inner horizon x_- (black) of the $\overline{\text{EMD}}$ and $\overline{\text{EMD}}$ black holes for three values of γ : $\gamma = -0.5$ (dash-dot), $\gamma = 0$ (dash) and $\gamma = 0.5$ (solid).

The photon sphere x_{ps} , the event horizon x_+ and the inner horizon x_- of the $\overline{\text{EMD}}$ and $\overline{\text{EMD}}$ black holes are displayed on Fig. 2. In the $\overline{\text{EMD}}$ case (Q/M) is restricted from above. When $\gamma < 0$ the inner "horizon" x_- is behind the central singularity and is not present on the figure. There are no constraints on (Q/M) for the $\overline{\text{EMD}}$ black hole. In non of the two cases with phantom scalar field the photon sphere and the event horizon merge.

3.2 Einstein Maxwell Dilaton black holes

The lens parameters a , b and u_{ps} for EMD case are given on Fig. 3. The observables are given on Fig. 4. The dashed line represents the critical curves of the parameters. For example, the critical curve for a is defined as $a_{\text{crit}}(\gamma) = a((Q/M)_{\text{crit}}, \gamma)$, where $(Q/M)_{\text{crit}}$ is the critical value of (Q/M) for the corresponding class of black-hole solutions. The critical curves of all other quantities in the paper are defined analogously and are represented by thin dashed lines.

Due to the electromagnetic charge the images are closer to the black hole. Their brightness decreases with the increase of Q/M and γ . The separation between them, however, increases as Q/M and γ are increased.

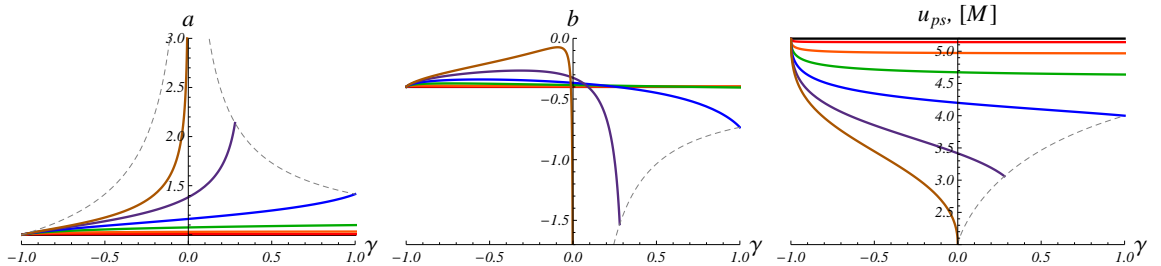


Figure 3: The EMD lens parameters a , b and u_{ps} for the following values of Q/M : $Q/M = 0$ (black), $Q/M = 0.25$ (red), $Q/M = 0.5$ (orange), $Q/M = 0.75$ (green), $Q/M = 1$ (blue), $Q/M = 1.25$ (purple), $Q/M = \sqrt{2}$ (brown).

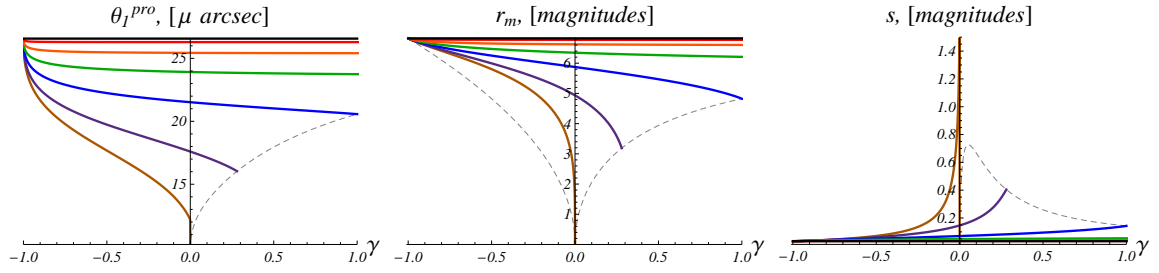


Figure 4: The observables θ_1^{pro} , r_m and s_1^{pro} for the EMD black hole. The values of Q/M are the same as on Fig. 3.

3.3 Einstein anti-Maxwell Dilaton black holes

The results for the $\overline{\text{EMD}}$ case are presented on Figs. 5 and 6. In this case the effect of the electromagnetic charge is to repel the images from the black hole. They become brighter but the separation between them is decreased. These effects become more appreciable as γ is decreased.

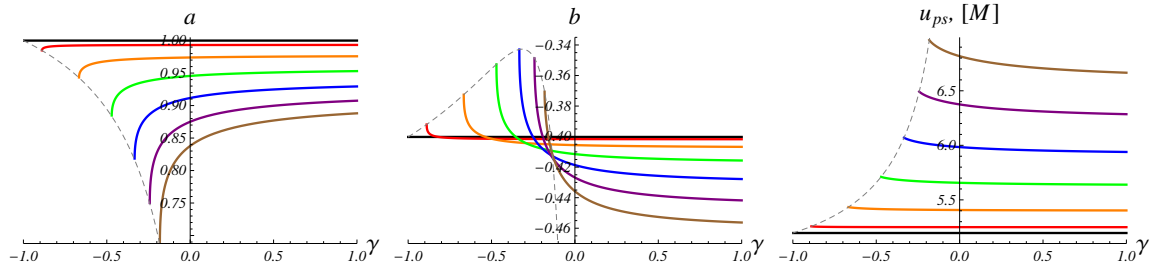


Figure 5: The $\overline{\text{EMD}}$ lens parameters a , b and u_{ps} for the following values of Q/M : $Q/M = 0$ (black), $Q/M = 0.25$ (red), $Q/M = 0.5$ (orange), $Q/M = 0.75$ (green), $Q/M = 1$ (blue), $Q/M = 1.25$ (purple), $Q/M = 1.5$ (brown).

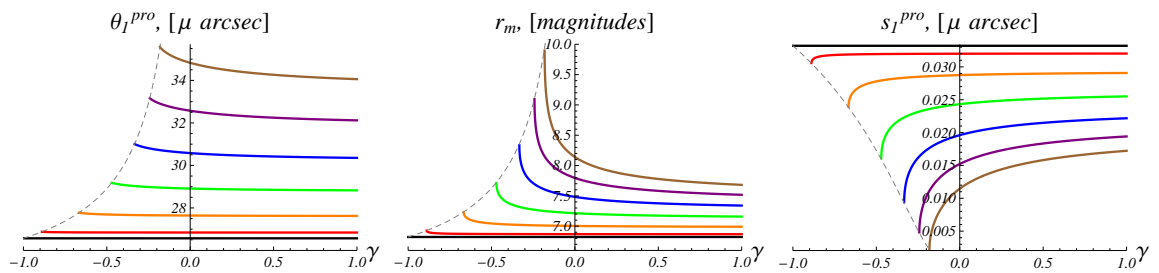


Figure 6: The observables θ_1^{pro} , r_m and s_1^{pro} for the $\overline{\text{EMD}}$ black hole. The values of Q/M are the same as on Fig. 5.

3.4 Einstein Maxwell anti-Dilaton black holes

The lens parameters and the observable in the case of $\overline{\text{EMD}}$ are presented on Figs. 7 and 8, respectively. With the increase of electric charge Q/M the angular position and the magnification of the images decrease while the separation between them increases. The angular positions seem to be slightly dependent on γ while the behavior of the two later observables becomes more appreciable as γ approaches -1 .

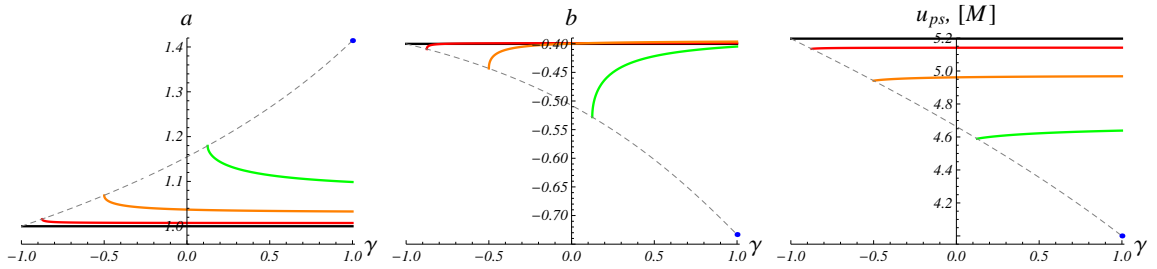


Figure 7: The $\overline{\text{EMD}}$ lens parameters a , b and u_{ps} for the following values of Q/M : $Q/M = 0$ (black), $Q/M = 0.25$ (red), $Q/M = 0.5$ (orange), $Q/M = 0.75$ (green), $Q/M = 1$ (blue).

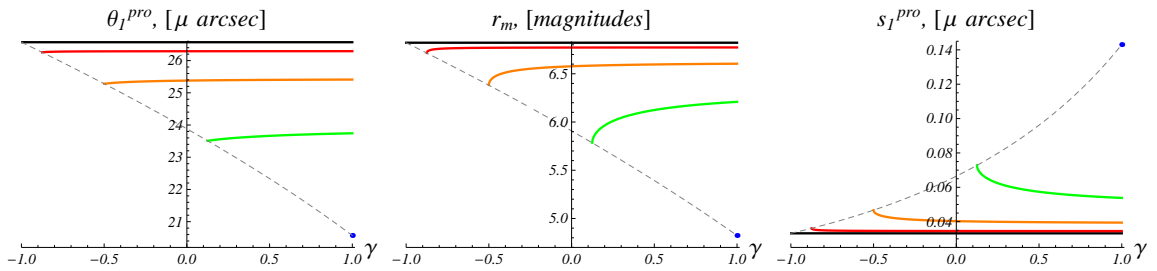


Figure 8: The observables θ_1^{pro} , r_m and s_1^{pro} for the $\overline{\text{EMD}}$ black hole. The values of Q/M are the same as on Fig. 7.

3.5 Einstein anti-Maxwell anti-Dilaton black holes

Figs. 9 and 10 represent the results for the last case – the $\overline{\text{EMD}}$ black hole. As we mentioned above, in this case there are no restrictions for the electric charge so no critical curves occur on the graphics. With the increase of electric charge Q/M the angular position and the magnification of the images increase while the separation between them decreases. Unlike the two previous cases the effect of the electric charge Q/M becomes less appreciable as γ approaches -1 .

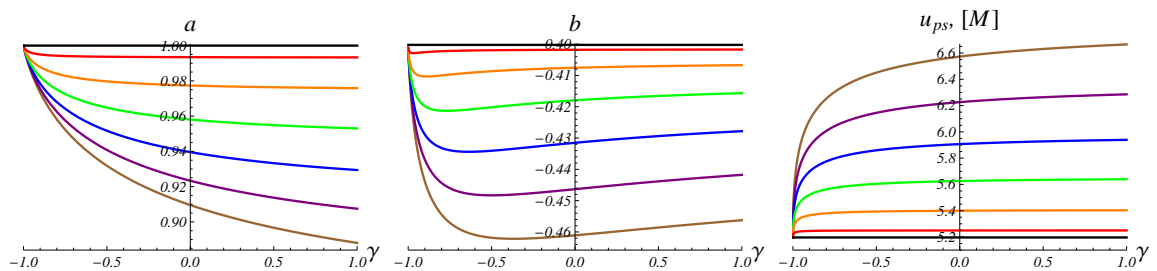


Figure 9: The $\overline{\text{EMD}}$ lens parameters a , b and u_{ps} for the following values of Q/M : $Q/M = 0$ (black), $Q/M = 0.25$ (red), $Q/M = 0.5$ (orange), $Q/M = 0.75$ (green), $Q/M = 1$ (blue), $Q/M = 1.25$ (purple), $Q/M = 1.5$ (brown).

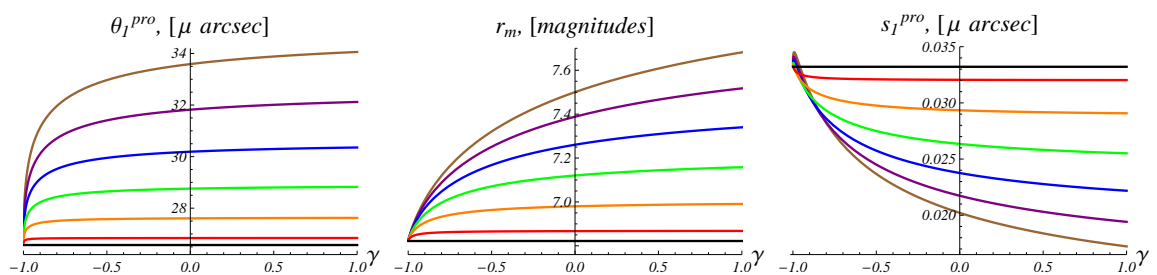


Figure 10: The observables θ_1^{pro} , r_m and s_1^{pro} for the $\overline{\text{EMD}}$ black hole. The values of Q/M are the same as on Fig. 9.

4 Comparison between the four cases and summary of the results

In this section we will compare between the four cases – (EMD), ($\overline{\text{EMD}}$), (EMD) and ($\overline{\text{EMD}}$) – for black holes with same mass M and electric charge Q . For all of the discussed cases on the same plot the photon sphere x_{ps} is presented on Fig. 11, the lens parameters a and b – on Figs. 12, the impact parameter and u_{ps} are on Figs. 13, and the other two observables, r_m and s_1^{pro} , are given on Figs. 14. On all graphics in the current section $M = 1$ and $Q = 0.8$.

The photon sphere plays a significant role for the formation of relativistic images. In all four cases it is present for the entire range of admissible values of the parameters – M , Q and γ .

Let us first compare between the effects of the Maxwell field and anti-Maxwell field on the relativistic images. The Maxwell field attracts the images. Due to the electromagnetic field they are closer to the black hole in comparison to the Schwarzschild case and less bright. The separation between the images of different order, the first and the second relativistic image in particular, however, is increased. The phantom (anti-Maxwell) electromagnetic field has an opposite effect. The images are repelled from the black hole and brighter but the separation between them is decreased. In both cases the effects become more significant with the increase of the electromagnetic charge and remain valid for all values of the parameter γ .

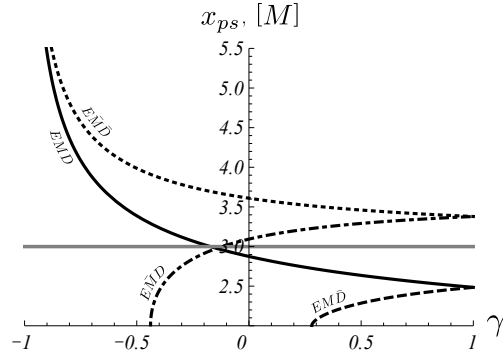


Figure 11: The photon sphere for $Q/M = 0$ corresponding to the Schwarzschild black hole (grey) and $Q/M = 0.8$ for the other four cases – EMD (thick), $\overline{\text{EMD}}$ (dash-dot), $\widetilde{\text{EMD}}$ (dash), $\overline{\text{EMD}}$ (dot).

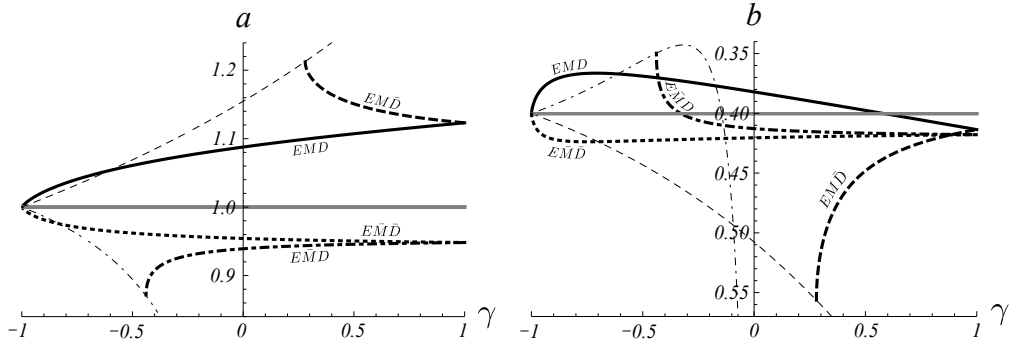


Figure 12: The lens parameters a and b for $Q/M = 0$ corresponding to the Schwarzschild black hole (grey) and $Q/M = 0.8$ for the other four cases – EMD (thick), $\overline{\text{EMD}}$ (dash-dot), $\widetilde{\text{EMD}}$ (dash), $\overline{\text{EMD}}$ (dot).

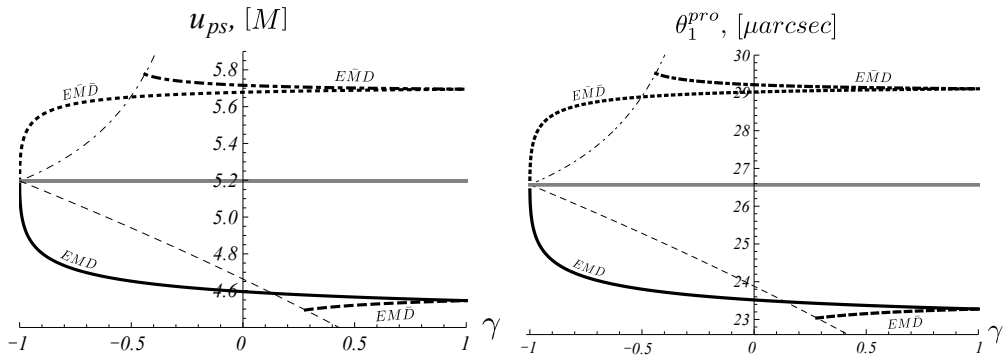


Figure 13: The impact parameter u_{ps} and the angular position of the first relativistic image for prograde photons θ_1^{pro} for $Q/M = 0$ corresponding to the Schwarzschild black hole (grey) and $Q/M = 0.8$ for the other four cases – EMD (thick), $\overline{\text{EMD}}$ (dash-dot), $\widetilde{\text{EMD}}$ (dash), $\overline{\text{EMD}}$ (dot).

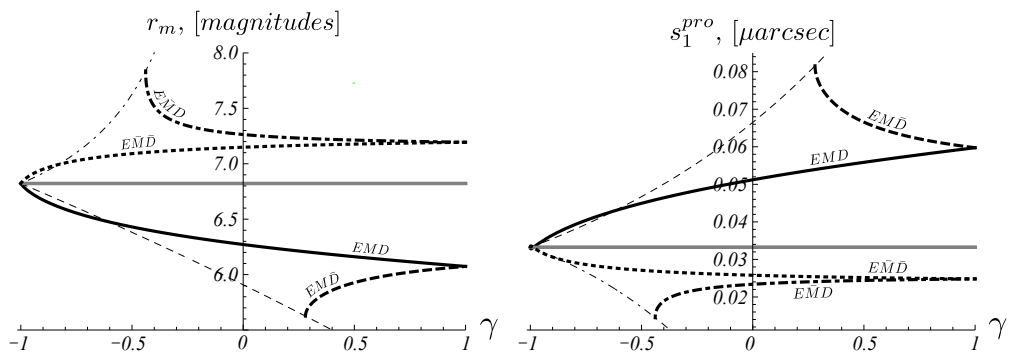


Figure 14: The flux ratio r_m and the angular separation between the first and second relativistic image for prograde photons s_1^{pro} for $Q/M = 0$ corresponding to the Schwarzschild black hole (grey) and $Q/M = 0.8$ for the other four cases – EMD (thick), $\overline{\text{EMD}}$ (dash-dot), $\widetilde{\text{EMD}}$ (dash), δEMD (dot).

Now let us compare between the canonical and phantom scalar fields. From the numerical results presented above we can conclude that due to the presence of the phantom scalar field the images are attracted to the horizon, demagnified and the separation between them is increased. The canonical scalar field yields an opposite effect.

As we can see in the different cases the images are either attracted to or repelled from the black hole. The numerical results do not show any tendency of this type for the photon sphere, however.

Acknowledgments

Partial financial support from the Bulgarian National Science Fund under Grant DMU 03/6 is gratefully acknowledged. The authors would like to thank prof. S. Yazadjiev for the fruitful discussions.

References

- [1] S. Hannestad, Int. J. Mod. Phys. **A21**, 1938 (2006), arXiv:astro-ph/0509320v2.
- [2] J. L. Tonry et al., Astrophys. J. **594**, 1 (2003), arXiv:astro-ph/0305008.
- [3] N. Jarosik et al. Astrophys. J. Suppl. **192**, 14 (2011), arXiv:1001.4744v1 [astro-ph.CO].
- [4] Miao Li, Xiao-Dong Li, Shuang Wang, Yi Wang, Commun. Theor. Phys. **56**, 525 (2011), arXiv:1103.5870v6 [astro-ph.CO].
- [5] Sh. Tsujikawa, invited review chapter on dark energy for a book "Dark Matter and Dark Energy: a Challenge for the 21st Century", Astrophysics and Space Science Library, 1, Volume 370, Dark Matter and Dark Energy, Part III, Pages 331-402, arXiv:1004.1493v1 [astro-ph.CO].

- [6] S. S. Yazadjiev and D. D. Doneva JCAP03(2012)037, arXiv:1112.4375.
- [7] S. S. Yazadjiev, Phys. Rev. **D83**, 127501 (2011), arXiv:1104.1865.
- [8] G. W. Gibbons, D. A. Rasheed, Nucl. Phys. **B476**, 515 (1996), arXiv:hep-th/9604177.
- [9] G. Clément, J. C. Fabris, M. E. Rodrigues, Phys. Rev. **D79**, 064021 (2009), arXiv:0901.4543v2 [hep-th].
- [10] , M. Azreg-Ainou, G. Clément, J. C. Fabris, M. E. Rodrigues, Phys. Rev. **D83**, 124001 (2011), arXiv:1102.4093 [hep-th].
- [11] C.J.Gao, S.N.Zhang, *Phantom Black Holes*, arXiv:hep-th/0604114.
- [12] K.A. Bronnikov, J.C. Fabris, Phys. Rev. Lett. **96**, 251101 (2006), arXiv:gr-qc/0511109.
- [13] M. E. Rodrigues, Z. A. A. Oporto, Phys. Rev. **D85**, 104022 (2012), arXiv:1201.5337v3 [gr-qc].
- [14] D. F. Jardim, M. E. Rodrigues, M. J. S. Houndjo, arXiv:1202.2830v2 [gr-qc].
- [15] A. Nakonieczna, M. Rogatko, R. Moderski, Phys. Rev. **D86**, 044043 (2012), arXiv:1209.1203 [hep-th].
- [16] M. Azreg-Ainou, *Light paths of normal and phantom Einstein-Maxwell-dilaton black holes*, arXiv:1209.5232 [gr-qc].
- [17] C. R. Keeton and A. O. Petters, Phys. Rev. **D72**, 104006 (2005).
- [18] V. Bozza, Phys. Rev. **D 66**, 103001 (2002).
- [19] V. Bozza, G. Scarpetta, Phys. Rev. **D76**, 083008 (2007), arXiv:0705.0246 [gr-qc].
- [20] A. Bhadra, Phys. Rev. **D67**, 103009 (2003), arXiv:gr-qc/0306016.
- [21] N. Mukherjee, A. S. Majumdar, Gen. Rel. Grav. **39**, 583 (2007), arXiv:astro-ph/0605224.
- [22] T. Ghosh, S. Sengupta, Phys. Rev. **D81**, 044013 (2010), arXiv:1001.5129v2 [gr-qc].
- [23] R. Whisker, Phys. Rev. **D71** 064004 (2005), arXiv:astro-ph/0411786.
- [24] E. F. Eiroa, Phys. Rev. **D73**, 043002 (2006), arXiv:gr-qc/0511065v2.
- [25] G. N. Gyulchev, S. S. Yazadjiev, Phys. Rev. **D75**, 023006 (2007), arXiv:gr-qc/0611110.
- [26] E. F. Eiroa, C. M. Sendra, Class. Quant. Grav. **28**, 085008 (2011), arXiv:1011.2455v2 [gr-qc].
- [27] Ch. Ding, J. Jing, JHEP **10**, 052 (2011), arXiv:1106.1974v2 [gr-qc].

- [28] J. Sadeghi, A. Banijamali, H. Vaez, *Strong Gravitational Lensing in a Charged Squashed Kaluza- Klein Black hole*, arXiv:1205.0805.
- [29] A. Y. Bin-Nun, Phys. Rev. **D82**, 064009 (2010), arXiv:1004.0379v2 [gr-qc].
- [30] Z. Horvath, L. A. Gergely, *Black hole tidal charge constrained by strong gravitational lensing*, arXiv:1203.6576v1 [gr-qc].
- [31] A. Y. Bin-Nun, Phys. Rev. **D81**, 123011 (2010), arXiv:0912.2081v2 [gr-qc].
- [32] L. Chetouani and G. Clément, Gen. Relativ. Gravit. **16**, 111 (1984).
- [33] J. G. Cramer, R. L. Forward, M. S. Morris, M. Visser, G. Benford, G. A. Landis, Phys.Rev. **D51** 3117 (1995), arXiv:astro-ph/9409051.
- [34] M. Safonova, D. F. Torres, G. E. Romero, Phys. Rev. **D65**, 023001 (2002), arXiv:gr-qc/0105070.
- [35] M. Safonova, D. F. Torres, Mod. Phys. Lett. **A17**, 1685 (2002), arXiv:gr-qc/0208039.
- [36] V. Perlick, Phys. Rev. **D69**, 064017 (2004), arXiv:gr-qc/0307072.
- [37] A. Shatskiy, Astron. Rep. **48**, 7 (2004), arXiv: astro-ph/0407222.
- [38] K. K. Nandi, Y. Z. Zhang, A. V. Zakharov, Phys. Rev. **D74**, 024020 (2006), arXiv:gr-qc/0602062.
- [39] T. K. Dey, S. Sen, Mod. Phys. Lett. **A23**, 953 (2008), arXiv:0806.4059v1 [gr-qc].
- [40] M. B. Bogdanov, A. M. Cherepashchuk, Astrophys. Space Sci. **317**, 181 (2008), arXiv:0807.2774v1 [astro-ph].
- [41] F. Abe, Ap. J. **725**, 787 (2010), arXiv:1009.6084v2 [astro-ph.CO]
- [42] Y. Toki, T. Kitamura, H. Asada, F. Abe, Ap. J. **740**, 121 (2011), arXiv:1107.5374v1 [astro-ph.CO].
- [43] N. Tsukamoto, T. Harada, K. Yajima, arXiv:1207.0047v1 [gr-qc].
- [44] K.S. Virbhadra , D. Narasimha, S.M. Chitre, Astron. Astrophys. **337**, 1 (1998), astro-ph/9801174 [astro-ph].
- [45] K. S. Virbhadra, G. F. R. Ellis, Phys. Rev. **D65**, 103004 (2002).
- [46] K.S. Virbhadra, C.R. Keeton, Phys. Rev. **D77**, 124014 (2008), arXiv:0710.2333 [gr-qc].
- [47] K. Sarkar, A. Bhadra, Class. Quant. Grav. **23**, 6101 (2006), arXiv:gr-qc/0602087.
- [48] G. N. Gyulchev, S. S. Yazadjiev, Phys. Rev. **D78**, 083004 (2008), arXiv:0806.3289 [gr-qc].

- [49] C.-M. Claudel , K.S. Virbhadra, G.F.R. Ellis, J. Math. Phys. **42**, 818 (2001),arXiv:gr-qc/0005050
- [50] P. P. Pradhan, *ISCOs in Extremal Gibbons-Maeda-Garfinkle-Horowitz-Strominger Blackholes*, arXiv:1210.0221 [gr-qc].